JACS
JOURNAL OF THE AMERICAN CHEMICAL SOCIETY
pubs.acs.org/JACS
Article

Buckyball-Based Spherical Display of Crown Ethers for *De Novo* Custom Design of Ion Transport Selectivity

Ning Li, Feng Chen, Jie Shen, Hao Zhang, Tianxiang Wang, Ruijuan Ye, Tianhu Li, Teck Peng Loh, Yi Yan Yang, and Huaqiang Zeng*

Cite This: *J. Am. Chem. Soc.* 2020, 142, 21082–21090
Read Online
ACCESS | Metrics & More | Article Recommendations | Supporting Information

ABSTRACT: Searching for membrane-active synthetic analogues that are structurally simple yet functionally comparable to natural channel proteins has been of central research interest in the past four decades, yet custom design of the ion transport selectivity still remains a grand challenge. Here we report on a suite of buckyball-based molecular balls (**MBs**), enabling transmembrane ion transport selectivity to be custom designable. The modularly tunable **MB*m*-C*n*** (m = 4−7; n = 6−12) structures consist of a C_{60}-fullerene core, flexible alkyl linkers C*n* (i.e., C6 for *n*-C_6H_{12} group), and peripherally aligned benzo-3*m*-crown-*m* ethers (i.e., m = 4 for benzo-12-crown-4) as ion-transporting units. Screening a matrix of 16 such **MBs**, combinatorially derived from four different crown units and four different C*n* linkers, intriguingly revealed that their transport selectivity well resembles the intrinsic ion binding affinity of the respective benzo-crown units present, making custom design of the transport selectivity possible. Specifically, **MB4s**, containing benzo-12-crown-4 units, all are Li^+-selective in transmembrane ion transport, with the most active **MB4-C10** exhibiting an $EC_{50}(Li^+)$ value of 0.13 μM (corresponding to 0.13 mol % of the lipid present) while excluding all other monovalent alkali-metal ions. Likewise, the most Na^+ selective **MB5-C8** and K^+ selective **MB6-C8** demonstrate high Na^+/K^+ and K^+/Na^+ selectivity values of 13.7 and 7.8, respectively. For selectivity to Rb^+ and Cs^+ ions, the most active **MB7-C8** displays exceptionally high transport efficiencies, with an $EC_{50}(Rb^+)$ value of 105 nM (0.11 mol %) and an $EC_{50}(Cs^+)$ value of 77 nM (0.079 mol %).

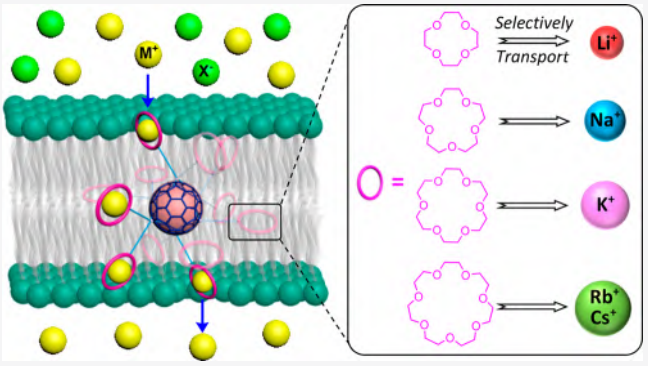

INTRODUCTION

Transmembrane transport of metal cations exquisitely regulated by natural channel proteins is ubiquitous in nature, which underlies diverse physiological processes to sustain life.[1−3] Significant progress has been made in recent years in revealing the structural conformation of these naturally evolved biomacromolecules and also in understanding the mechanism by which they can traffic ion flux efficiently and selectively.[4−7] Such knowledge has further enabled and inspired scientists, especially synthetic chemists, to design artificial versions of functional ion transporters that not only deepen our understanding of transmembrane transport but also pave the way for their potential applications in the pharmaceutical and chemical industries.[8−16]

In most biological systems, Na^+ and K^+ perform in combination as the electrolyte in both intra- and extracellular environments, exerting pivotal regulatory roles in vital physiological functions such as muscle contraction, neural signal transmission, and heartbeat. To perform such functions properly, these cations have to move across the intrinsically impermeable cell membrane in both an efficient and selective manner. This is exactly what nature has achieved using evolutionally selected protein channels. For instance, the KscA channel, as one of the most well-studied membrane-embedded natural channel proteins, can transport ~10^8 K^+ ions per second, with an extraordinarily high K^+/Na^+ selectivity of ~10000.[4] In the field of synthetic cation transporters, exciting advancement has been achieved regarding the transport efficiency on par with the natural systems,[17] but devising artificial transporters with high and designable cation selectivity still represents a daunting task for the research community.

Crown ethers (CEs), discovered in the late 1960s,[18] have been experiencing extensive investigative efforts for the design of a plethora of artificial membrane transporters over the last few decades.[17,19−28] This is primarily built upon their structural simplicity and unique coordination capability toward

Received: September 8, 2020
Published: December 4, 2020

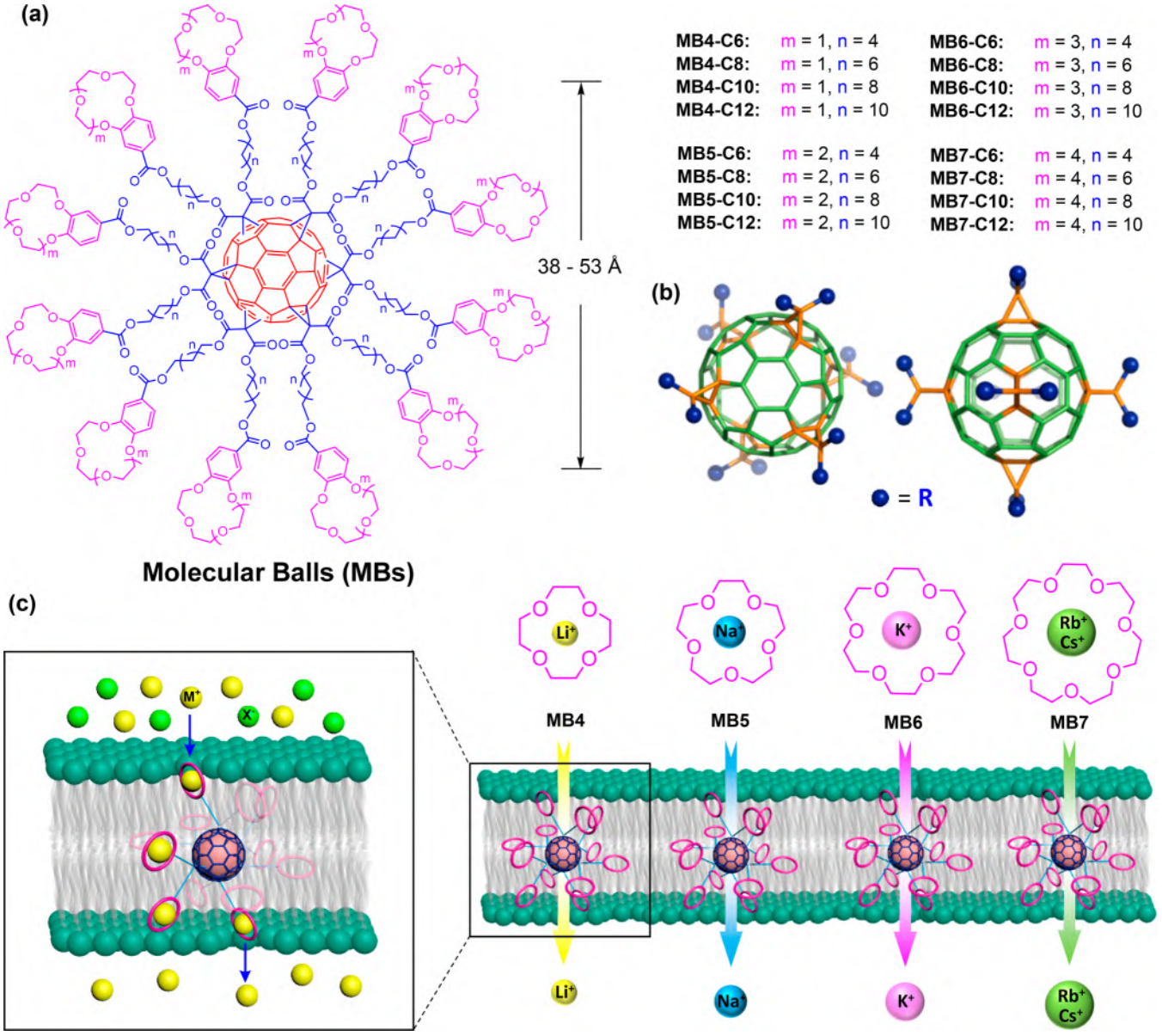

Figure 1. Molecular design of buckyball-based molecular balls as ion-selective transporters. (a) Molecular structures of designed **MB**s with diversifications in flexible alkyl linker lengths and peripheral crown ether units for a combinatorial identification of selective and efficient **MB**s. (b) Illustrations of **MB**'s three-dimensional configuration and distribution of 12 side arms. (c) Schematic illustration of **MB**s participating in transmembrane transport of alkali-metal ions with selectivity imparted by the crown ether's intrinsic ion-binding selectivity, with the proposed ion transport mechanism shown in the square box on the left.

the biologically relevant alkali-metal ions. Although numerous studies have shown that binding of CEs with alkali-metal ions in solution largely follows the so-called size-fit rule (i.e., 12-crown-4, 15-crown-5, 18-crown-6, and 21-crown-7 favoring Li^+, Na^+, K^+, and Cs^+ ions, respectively)[29−33] such a trend was found to be absent in many other examples.[34] Specifically in the realm of synthetic ion transporters, it is also impractical to reliably predict the ion transport selectivity of the CE-based transporters from their solution binding profile.[17,19,20,24,25] Intuitively, favorable ion binding should benefit the ion-capturing process but could be detrimental to ion release to the next binding site or the other side of the membrane. For example, a number of 15-crown-5-based synthetic transporters were found to be capable of selectively transporting K^+ ions, instead of Na^+.[17,19,20,24] Similarly, Barboiu and co-workers revealed a transport selectivity order of $Cs^+ > Rb^+ > K^+ > Na^+ > Li^+$ for H-bond-directed stacks of 18-crown-6, largely deviating from their solution binding affinities.[24] Previous studies on Cl^- anionophores have shown that the tight-binding-associated retarding effect is not predictable either, in which anionophores of higher Cl^- binding affinity can lead to backbone-dependent higher[35] or lower[36] transport efficiencies and hence selectivities. Therefore, it would be of high interest and value to identify ion-transporting scaffolds that could facilitate a direct translation of solution binding affinity to transmembrane ion transport selectivity without compromising the transport efficiency.

Herein we present such a distinctive class of C_{60}-fullerene-based molecular balls (**MB**s, Figure 1a) carrying CEs on the periphery and exhibiting excellent transport selectivity toward alkali-metal ions that closely follows the CE ion binding affinity in solution. In particular, upon insertion into a lipid membrane,

https://dx.doi.org/10.1021/jacs.0c09655
J. Am. Chem. Soc. 2020, 142, 21082−21090

MB4-C10 containing 12 benzo-12-crown-4 units and *n*-C**10**H_{20} linkers allows Li^+ to rapidly pass through while excluding nearly all other monovalent alkali-metal ions. Similarly, **MB5-C8**, **MB6-C12**, and **MB7-C8** exhibit good to excellent transport selectivities toward Na^+, K^+, and Rb^+/Cs^+ ions, respectively. In addition, these **MB**s also display high transport efficiency, with EC_{50} values in the range of 0.079−0.48 mol % relative to lipid molecules present in the membrane. Analogous supramolecular spherical assemblies have attracted extensive interest in diverse fields such as gene delivery and regulation,[37−39] protein binding,[40] and antiviral activity.[41] To this end, our unique design of **MB**s as synthetic ion transporters offers an unprecedented approach toward attaining both high transport efficiency and especially custom designable ion selectivity, an unmet challenge that has been long sought after.

RESULTS AND DISCUSSION

The structure of these **MB**s is modularly tunable, consisting of a C_{60}-fullerene core, flexible alkyl linkers, and CEs as the ion capture and transport units at the molecular periphery (Figure 1a). Four types of CEs were selected in this study, i.e., 12-crown-4, 15-crown-5, 18-crown-6, and 21-crown-7, as they are known to favorably bind with alkali-metal ions from Li^+ to Cs^+ (ionic radius of 0.76−1.67 Å) via host−guest complexation.[33] In experiments using the chloroform−water biphasic picrate extraction method developed by Cram,[42] we obtained the binding constants of the corresponding benzo versions, i.e., benzo-12-crown-4, -15-crown-5, -18-crown-6, and -21-crown-7, revealing their preferential binding with Li^+, Na^+, K^+, and Cs^+/Rb^+ ions (Scheme S4 and Table S1), respectively. Alkyl chains were then used to link the fullerene core and the benzo-CE units, in order to establish the structural flexibility and also to enhance the lipophilicity of the **MB**. Since linkers may affect the transport performance,[17,21] we further screened four alkyl chains of different lengths (i.e., *n*-C_6H_{12}, *n*-C_8H_{16}, *n*-$C_{10}H_{20}$, and *n*-$C_{12}H_{24}$), giving **MB**s with estimated physical diameters of 38−53 Å at their most extended state (excluding the amphiphilic CEs, Figure 1a). They are dimensionally comparable to the thickness of typical lipid bilayer membranes, usually about 30−35 Å thick for the hydrophobic region and 50−55 Å overall, including the polar head groups and midpolar regimes.[28]

The actual synthesis of these **MB**s was accomplished via three steps, including (i) reacting bromo alcohols with malonic acid to obtain the V-shaped alkyl linkers, (ii) attaching such linkers onto C_{60}-fullerene via the Bingel reaction in a 6:1 ratio, and (iii) introducing 12 CE units at the molecular periphery to complete the sphere construction. The Bingel addition of malonates onto the fullerene core is octahedrally symmetric, giving **MB**s with 12 CE units evenly distributed on the surface (Figure 1b). In total, a matrix of 16 **MB**s (combination of four linkers and four CEs, expected molecular weight in the 5534−8128 Da range) were prepared. Although their identity and high purity of >90% could be confidently confirmed by HPLC (Figure S1) and ^1H and ^{13}C NMR spectroscopy (Figure 2 and Figure S2 as well as spectra in the Supporting Information), the possibility of incomplete functionalization of C_{60}-fullerene cannot be exclusively ruled out. No molecular peaks were observed in the MALDI-TOF mass spectra, suggesting their easy fragmentation under laser beam irradiation. It is worth noting that **MB4**s, **MB5**s, and some of the **MB6**s with short linkers (**MB6-C6**, **MB6-C8**, and **MB6-C10**) are dark solids,

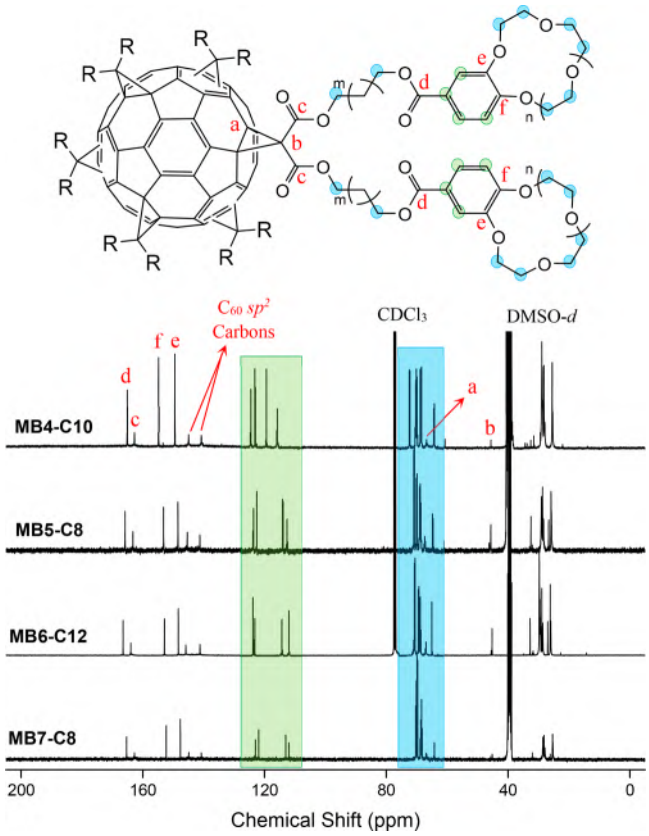

Figure 2. ^{13}C NMR spectra of **MB4-C10**, **MB5-C8**, **MB6-C12**, and **MB7-C8** in DMSO-*d* or $CDCl_3$. Representative signals assigned and labeled are in full agreement with the octahedral symmetry of the molecules.

whereas **MB6-C12** and all **MB7**s are tarlike heavy oils. These **MB**s are found to be soluble in chloroform, dichloromethane, dimethylformamide, and dimethyl sulfoxide but only poorly soluble in acetonitrile or methanol.

In the literature, ^{13}C NMR spectroscopy has been established as a particularly useful tool for the structure characterization and purity confirmation of C_{60}-fullerene hexakis adducts, as two signatory signals of the sp^2 carbons of C_{60} can usually be observed, in accordance with the octahedral symmetry of the C_{60} core.[37,43] The spectrum of **MB4-C10**, for example, shows such sp^2 signals at δ 140.8 and 145.0 ppm (Figure 2 and Figure S2). The C_{60} sp^3 carbon and the malonate bridgehead carbon signals emerge at δ 66.8 and 45.7 ppm, respectively. In addition, two carbonyl signals (δ 165.1 and 162.7 ppm) were also observed, which are in full consistency with the proposed octahedral molecular symmetry. Similar ^{13}C NMR spectra were obtained for all other **MB**s as well, and their ^1H NMR spectra also display a full set of expected signals with satisfactory integration ratios, although the peak multiplicity is lost in some cases (see the Supporting Information for more details). In view of such highly symmetrical structures with flexible alkyl linkers and ion-capturing CEs, we envisioned that the appropriately sized **MB**s might be able to perform as efficient transporters to move alkali-metal ions across a lipid bilayer membrane in the presence of an ionic concentration gradient (Figure 1c).

The well-established fluorescence-based HPTS assay[44,45] was adapted in this study to assess the ion transport selectivity and efficiency of these **MB**s (Figure 3a). In this assay, large

https://dx.doi.org/10.1021/jacs.0c09655
J. Am. Chem. Soc. 2020, 142, 21082−21090

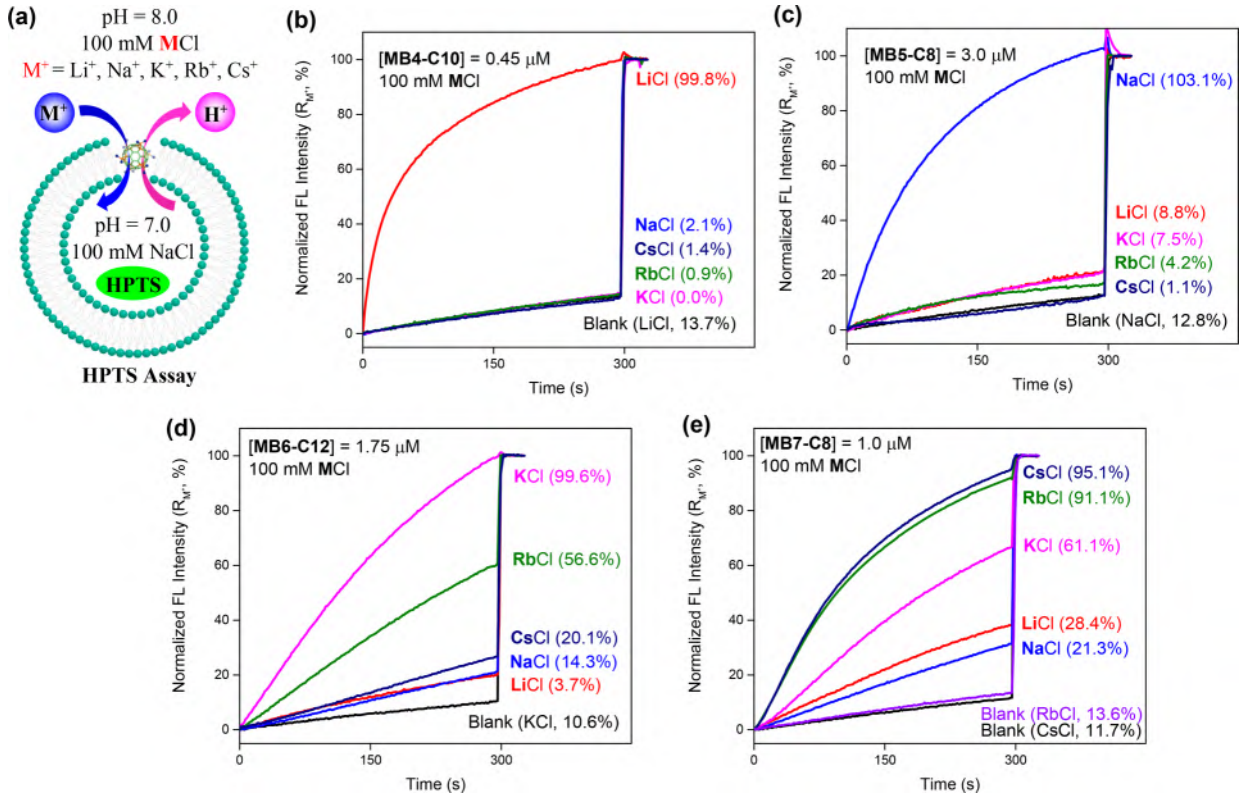

Figure 3. LUV-based lipid bilayer experiments for elucidating ion transport activity and selectivity. (a) Schematic illustration of the pH-sensitive HPTS assay for ion transport study. Different extravesicular salts are used to facilitate the comparison of ion transport activities. (b–e) M^+ ion transport selectivity of the most active **MB**s in each subgroup selective to different alkali-metal ions, determined over 300 s with an extravesicular environment of 100 mM MCl (M^+ = Li^+, Na^+, K^+, Rb^+, Cs^+): (b) for **MB4-C10**; (c) for **MB5-C8**; (d) for **MB6-C12**; (e) for **MB7-C8**. The normalized fluorescence intensity R_{M^+} is calculated by the formula $R_{M^+} = (I_{M^+} - I_0)/(I_{Triton} - I_0)$, in which I_{M^+} and I_{Triton} are the fluorescence intensities at 300 s before and after the Triton addition, respectively, and I_0 is the background intensity. While Blank (LiCl, 13.7%) in (b) means that the background transport percentage of Li^+ ion in absence of any **MB** is 13.7%, NaCl (2.1%) in (b) refers to a normalized ion transport activity value in the presence of the transporter **MB4-C10**, after subtracting the **MB4-C10**-mediated transport percentage of 14.6% from the background signal Blank (NaCl, 12.8%) and further normalization (e.g., 2.1% = (14.6% − 12.8%)/(100% − 12.8%)). [Total LUV lipid] = 97.5 μM.

unilamellar vesicles (LUVs; about 120 nm in diameter) were fabricated using EYPC (egg yolk L-α-phosphatidylcholine), trapping 10 mM HEPES buffer, 100 mM NaCl, and 1.0 mM pH-sensitive HPTS dye (8-hydroxyprene-1,3,6-trisulfonic acid) in the intravesicular region at pH 7.0. The extravesicular environment was set to be 100 mM MCl (M^+ = Li^+, Na^+, K^+, Rb^+, Cs^+) and 10 mM HEPES at pH 8.0. In such an asymmetric system, the pH gradient provides the driving force to move the alkali-metal ions toward the intravesicular region. This cation translocation is associated with either proton efflux or hydroxide influx for charge neutralization, resulting in an intravesicular pH increase that can be seen macroscopically by monitoring the fluorescence intensity of the encapsulated HPTS dye.

Initial screening using the HPTS assay revealed that all **MB**s are able to transport alkali-metal ions across the LUV membrane. More importantly, their transport selectivity is highly dependent on the choice of CE units in the molecular structure. The data compiled in Table 1 and Figure 3 show that those containing 12-crown-4 preferably transport Li^+, and the 15-crown-5-, 18-crown-6-, and 21-crown-7-containing **MB**s are selective to Na^+, K^+, and Rb^+/Cs^+ ions, respectively.

The classic Hill analyses were performed to determine the EC_{50} values for these **MB**s, at which 50% of the maximal transport activity is reached. As shown in Table 1, the majority show EC_{50} values of around 5.0 μM or below, indicating their good transport efficiency. The most efficient candidate in each subgroup selective to a particular alkali-metal ion was identified to be **MB4-C10**, **MB5-C8**, **MB6-C12**, and **MB7-C8**, and their $EC_{50}(M^+)$ value were determined as 0.13 μM, 0.47 μM, 0.40 μM, and 105 nM/77 nM for Li^+, Na^+, K^+ and Rb^+/Cs^+ ions, respectively.

Ion transport selectivity of these **MB**s can be quantified using the ratio of fractional transport activity R_{M^+} in the HPTS assay, given that R_{M^+} is obtained at the **MB** concentration where the activity for the most active ion reaches 95–100% over the 300 s data recording period. We and others have verified the reliability of such an R_{M^+}-based approach to ion selectivity quantification, with reference to the classic planar lipid bilayer method.[19,46] The selectivity profiles for the most efficient **MB4-C10**, **MB5-C8**, **MB6-C12**, and **MB7-C8** are shown in Table 1 and in Figure 3b–e. Similar patterns were also observed on other **MB**s containing respective CEs, although their ion-discriminating capabilities differ (Figures S3–S18).

At 0.45 μM, **MB4-C10**, containing Li^+-selective benzo-12-crown-4 units (Table S1) and n-$C_{10}H_{20}$ linkers, induces the maximal transport activity for Li^+ (R_{Li^+} = 99.8%), yet no obvious activity was seen for other alkali metal ions (R_{M^+} = 0–2.1%, M^+ = Na^+, K^+, Rb^+, Cs^+; Figure 3b). The transport selectivity, therefore, calculated by the R_{Li^+}/R_{M^+} ratio, was deemed to be greater than 47.5. In 2011, Otis et al. reported

https://dx.doi.org/10.1021/jacs.0c09655
J. Am. Chem. Soc. 2020, 142, 21082–21090

Table 1. Ion Transport EC_{50} Values (Half Maximal Effective Concentration, in μM) and Selectivities of All MBs Calculated from the EYPC-LUV Experimental Data Using Hill Analysis[d]

	MB4-C6	MB4-C8	MB4-C10	MB4-C12
$EC_{50}(Li^+)$[a]	2.87 ± 0.22	1.01 ± 0.11	**0.13 ± 0.01**	0.16 ± 0.01
Li^+/M^+[c]	2.4 - 3.6	14.3 - 18.1	≥ 47.5	18.2 - 56.7
	MB5-C6[b]	MB5-C8	MB5-C10	MB5-C12
$EC_{50}(Na^+)$[a]	> 7.5	**0.47 ± 0.06**	1.29 ± 0.10	1.62 ± 0.11
Na^+/K^+	3.7	13.7	10.6	4.5
	MB6-C6[b]	MB6-C8	MB6-C10	MB6-C12
$EC_{50}(K^+)$[a]	> 25	0.52 ± 0.05	0.86 ± 0.06	**0.40 ± 0.03**
K^+/Na^+	1.6	7.8	7.7	7.0
	MB7-C6	MB7-C8	MB7-C10	MB7-C12
$EC_{50}(Rb^+)$[a]	11.33 ± 1.86	**0.105 ± 0.006**	5.53 ± 0.47	5.03 ± 0.13
Rb^+/M^+[c]	2.5 - 10.2	1.5 - 4.3	1.1 - 5.1	1.4 - 29.7
$EC_{50}(Cs^+)$[a]	6.90 ± 1.06	**0.077 ± 0.006**	5.00 ± 0.42	4.77 ± 0.12
Cs^+/M^+[c]	2.9 - 11.8	1.6 - 4.5	1.0 - 4.6	1.4 - 30.9

[a]The calculation was accomplished by fitting the transport activity versus **MB** concentration using the Hill equation $Y = 1/(1 + (EC_{50}/[\mathbf{MB}])^n$, giving the EC_{50} values and Hill coefficient n. The R^2 values for all fittings were greater than 0.90. The total lipid concentration utilized was 97.5 μM in these tests. [b]EC_{50} values cannot be experimentally determined, as precipitations occur before 50% of the maximal transport activity is reached. [c]Li^+/M^+, Rb^+/M^+, and Cs^+/M^+ refer to the transport selectivity of Li^+, Rb^+ and Cs^+ over other alkali-metal ions, respectively. [d]The boldface entry in each row of $EC_{50}(M^+)$ represents the highest ion transport activity of **MB**s containing the same crown units but different alkyl linkers.

on a 12-crown-4-based helical peptide, but its Li^+ selectivity was not well characterized.[27] Lithium salts have been found to be effective in treating manic depression and also in reducing a patient's risk of attempting suicide,[47,48] whereas a major drawback of such lithium therapy is the low penetration rate of lithium through biological membranes. This leads to delayed onset and decreased effect of the pharmaceutical action, usually making relatively large doses necessary that could further cause undesirable side effects.[49] Given an $EC_{50}(Li^+)$ value of 0.13 μM and Li^+/M^+ selectivity of greater than 47.5, we anticipate that **MB4-C10** may have potential value as potent codrugs in such lithium therapy. Similar excellent Li^+ selectivity is also seen with **MB4-C8** and **MB4-C12**, although their transport efficiency varies with $EC_{50}(Li^+)$ values of 1.01 and 0.16 μM, respectively (Table 1). Other potential applications of such highly efficient, Li^+-selective synthetic transporters could include electrolytes for lithium batteries,[50] production of ion-selective electrodes,[51,52] lubricants,[53] and even extraction of lithium from the ocean.[54,55]

MB5-C8, containing Na^+-selective benzo-15-crown-5 (Table S1) and n-C_8H_{16} linkers, selectively transports Na^+ ions, giving a fractional activity R_{Na^+} of 103.1% at 3.0 μM (Figure 3c). Its corresponding R_{M^+} values for Li^+, K^+, Rb^+ and Cs^+ are 8.8%, 7.5%, 4.2%, and 1.1% respectively, indicative of an excellent Na^+ selectivity. In the literature, Na^+ transporters have been far less well-developed than K^+-selective transporters,[21,56,57] despite both being critically important electrolytes in biological systems. This is potentially due to the higher dehydration energy of Na^+ ions,[31,58] making its membrane penetration energetically less favorable in comparison to K^+ ions. Accordingly, many 15-crown-5-based transporters have demonstrated ion transport selectivity toward K^+, instead of Na^+.[17,19,20,24] Previously, a 15-crown-5-containing molecular ion fisher, consisting of a lipid anchoring cholesterol moiety (fishing rod), flexible alkyl chain (fishing line), and benzo-15-crown-5 unit (fish hook), was reported to be a selective CE-based Na^+ ion transporter.[21] It featured a low Na^+/K^+ selectivity of 3.6 and a low transport activity ($EC_{50}(Na^+)$ > 25% of the membrane lipid present). With a Na^+/K^+ selectivity of 13.7 and $EC_{50}(Na^+)$ value of 0.47 μM (0.48 mol % relative to lipid), this **MB5-C8** is undoubtedly among the best Na^+-selective synthetic transporters to date.[56,57,59] Such Na^+/K^+ selectivity is even comparable to that of some of the natural Na^+ channels.[60,61]

Following the same trend, the benzo-18-crown-6-containing **MB6-C12** shows excellent transport selectivity to K^+ ions (Figure 3d), attaining an R_{K^+} value of 99.6% at 1.75 μM. For comparison, R_{Na^+} obtained under identical experimental conditions is merely 14.3%, implying a K^+/Na^+ selectivity of 7.0. Although such selectivity is inferior to the highest example in the literature (18.0 for the molecular ion fisher design described above[21]), its transport efficiency (EC_{50} = 0.41 mol %) is about 2 times higher (EC_{50} = 1.1 mol % for the molecular ion fisher), making it an overall excellent K^+-selective synthetic transporter. As discussed earlier, favorable ion binding does not necessarily lead to superior ion transport selectivity for K^+ ions. For instance, Sun et al. reported on H-bond-directed stacks of cholesteryl-18-crown-6 complexes in 2015, which feature clear Cs^+ selectivity followed by Rb^+, K^+, Na^+, and Li^+ in descending order.[24] It is also worth mentioning that the K^+-selective **MB6-C12** displays K^+/Li^+, K^+/Cs^+, and K^+/Rb^+ selectivities of 26.9, 5.0 and 1.8, reminiscent of the MD simulation results of ion binding affinity of 18-crown-6 in aqueous solution.[31] A similar transport activity ($EC_{50}(K^+)$ = 0.52 and 0.86 μM) and K^+/Na^+ selectivity (R_{K^+}/R_{Na^+} = 7.8 and 7.7) can also be achieved with **MB6-C8** and **MB6-C10**, respectively (Table 1 and Figures S12 and S13). Together with **MB6-C12**, they form a group of highly active synthetic K^+ transporters with high K^+/Na^+ selectivity.

Likewise, **MB7-C8** containing 21-crown-7 as the ion capture unit favorably transports the large Rb^+ and Cs^+ ions with almost identical selectivity and efficiency (Figure 3e). In the literature, examples of 21-crown-7-based ion transporters are relatively rare, in comparison to other CEs. Voyer et al. once reported a 21-crown-7-appended helical peptide as an ion channel, which unfortunately is unable to differentiate alkali-metal ions.[26] Otis et al. also showed similar 21-crown-7-based α-helical peptides acting as transmembrane ion channels with a selectivity order of $Cs^+ > K^+ > Na^+$, despite their moderate transport efficiency.[27] In comparison, **MB7-C8** displays preferable transport of Cs^+ and Rb^+ ions (R_{Cs^+} = 95.1% and R_{Rb^+} = 91.1% at 1.0 μM), with Cs^+/K^+, Cs^+/Na^+, and Cs^+/Li^+ selectivities of 1.6, 4.5, and 3.3, respectively. The EC_{50} values of **MB7-C8** toward Rb^+ and Cs^+ ions, determined by Hill analysis, are 105 and 77 nM, respectively, corresponding to transporter/lipid ratios of about 1/928 and 1/1266, or 0.11 and 0.079 mol % relative to lipid. This makes **MB7-C8**, to the best of our knowledge, the most efficient Rb^+ and Cs^+ synthetic transporter to date.

https://dx.doi.org/10.1021/jacs.0c09655
J. Am. Chem. Soc. 2020, 142, 21082−21090

One may have noticed the differences in ion transport selectivity of **MB**s bearing the respective crown units described above (Figure 3b–e), which are well aligned with the solution binding selectivities of benzo-CEs (Table S1). In general, **MB**s containing small CEs (i.e., 12-crown-4 and 15-crown-5) demonstrate much better selectivity than those containing large CEs (i.e., 18-crown-6 and 21-crown-7). This trend agrees with previous observations that the binding affinity of different CEs toward their preferred alkali-metal ions was more pronounced for small ions in comparison to large ions.[33] The structural flexibility of the CE macrocycle may account for such an incongruity. Apart from the preferred ones, large CEs can readily deform and adapt their macrocycles for binding with small alkali-metal ions,[30] whereas the opposite situation (i.e., small CEs binding with large ions) is unlikely and might require alternative binding configurations, such as a sandwich-like complex involving two CEs and one cation.[30] This may explain the exceptional selectivity of **MB4-C10** for Li^+ and **MB5-C8** for Na^+ ions, followed by the high selectivity of **MB6-C8** for K^+ ions and the low selectivity of **MB7-C8** for Cs^+/Rb^+ ions (Table 1). To further shed light on the ion transport mechanism, we prepared the 18-crown-6-based control compound **MB6-R**, having a rigid 1,2,3-triazole moiety in the alkyl linker of ~14.4 Å (Figure S19). This length is comparable to that of *n*-C_6H_{12} (~13.2 Å) in **MB6-C6** and *n*-C_8H_{16} linkers (~15.6 Å) in **MB6-C8**. However, no detectable K^+ transport activity emerged with **MB6-R** at a concentration as high as 5.0 μM, while the similar-sized **MB6-C6** and **MB6-C8** exhibit transport activities of 46.3% and 100% at 5.0 and 2.5 μM, respectively (Figure S19). These comparative data clearly reveal the indispensable role of flexibility of the alkyl linkers for these **MB**s to perform as ion transporters. One possible ion transport pathway can therefore be proposed (Figure 1c), involving (i) ion capture at the membrane-water interface, (ii) ion relay between adjacent CEs facilitated by swinging of the flexible alkyl linker, and (iii) ion release upon reaching the opposite side.[62]

These **MB**s share certain similarities with both conventional channel- and carrier-class transmembrane ion transporters. On one hand, they span across the entire membrane with openings to both the intra- and extravesicular regions simultaneously, an inherent characteristic to channels. On the other hand, there exist no well-defined passages for ions to pass through and the transporting components (alkyl linkers and CEs) are free to move within certain regions of the lipid membrane, resembling how carriers ferry ions across. Single-channel current measurements were therefore carried out to determine which mechanism (channel or carrier) **MB** is following to transport alkali-metal ions. Despite the extensive efforts devoted, our failure to capture any single-current signals suggests that these **MB**s might perform more like ion carriers.

To confirm alkali-metal ions as the main transporting species, we introduced the chloride-sensitive SPQ (6-methoxy-*N*-(3-sulfopropyl) quinolinium) dye into the LUV-based assay (Figure 4a).[63] The intravesicular region contains 0.5 mM SPQ and 200 mM $NaNO_3$ salt, and the extravesicular environment is set to be 200 mM NaCl. To establish the efficacy of this SPQ assay, the previously reported anion channel **L8** was used as the positive control,[64] which caused 62.0% SPQ fluorescence quenching at 2.0 μM. At the same concentration, no detectable quenching was observed with **MB6-C12** or **MB7-C8**. Unfortunately, **MB4-C10** and **MB5-C8** precipitated out at 2.0 μM in the buffer-free salt solution. A lower concentration

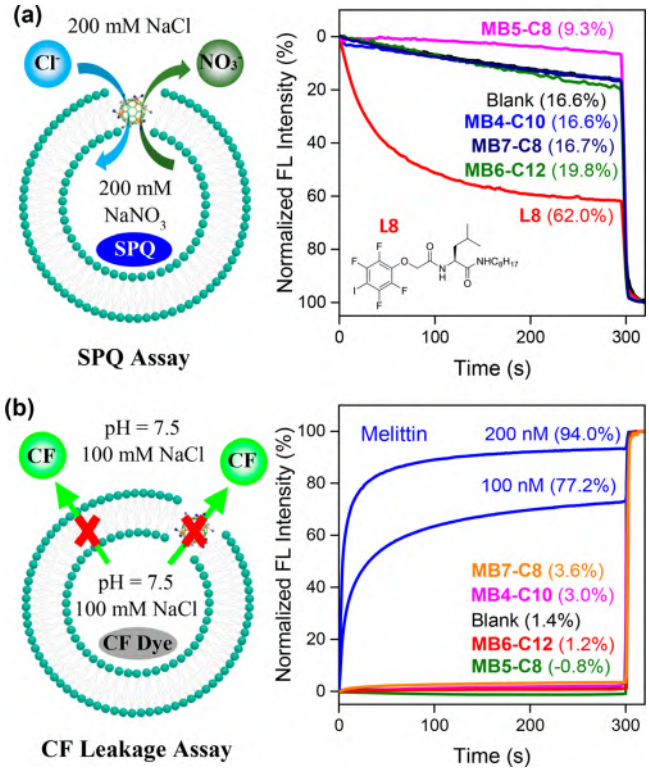

Figure 4. Schematic illustration and experimental results of SPQ and CF dye leakage assays. (a) SPQ assay to confirm the inability of **MB**s to transport Cl^- anions. [**MB6-C12**] = [**MB7-C8**] = [**L8**] = 2.0 μM; [**MB4-C10**] = [**MB5-C8**] = 0.1 μM. (b) CF dye leakage assay to confirm the LUV integrity in the presence of **MB**s at 2.0 μM.

of 0.1 μM was therefore utilized, at which **MB4-C10** and **MB5-C8** induced a fractional transport activity R_{Li^+} value of 34.9% and R_{Na^+} value of 19.4% in the HPTS assay, but no obvious SPQ fluorescence quenching was observed. When this is combined with the fact that these **MB**s are only weakly active for their unfavorable alkali-metal ions, the contradistinctive data clearly confirm the incapability of **MB**s to transport anions, and the M^+/H^+ antiport should be the main transporting species.

We further conducted a carboxyfluorescein (CF) dye leakage assay to confirm the LUV membrane integrity in the presence of these **MB**s (Figure 4b).[65] The CF-containing LUVs were prepared with the intravesicular region containing 50 mM CF dye, 10 mM HEPES, and 100 mM NaCl at pH 7.5. The extravesicular region only containsed HEPES and NaCl at identical pH. At such a high concentration, trapped CF dyes largely remain as nonfluorescent dimers, whereas a dramatic fluorescence increase will emerge if there is any CF dye leakage or membrane destruction taking place. As shown in Figure 4b, **MB4-C10**, **MB5-C8**, **MB6-C12**, and **MB7-C8** at 2.0 μM do not induce any fluorescence increase, and a similar conclusion can also be drawn for other **MB**s (Figure S20). Conversely, melittin, a pore-forming peptide as the positive control in this assay, causes significant fluorescence increases of 77.2% and 94.0% at lower concentrations of 100 and 200 nM, respectively. These results unambiguously confirm that the LUV membrane integrity is maintained in the presence of **MB**s and that the ion transport activities observed are not due to any **MB**-induced membrane-lysing effect.

https://dx.doi.org/10.1021/jacs.0c09655
J. Am. Chem. Soc. 2020, 142, 21082–21090

CONCLUSIONS

In summary, we have successfully prepared a suite of modularly structured buckyball-based molecular balls and for the first time demonstrated that solution-based cation binding selectivity can be reliably translated into membrane-based transport selectivity. More precisely, identified to be the most active in their respective group containing the same crown units (EC_{50} = 0.079−0.48 mol % relative to lipid molecules), **MB4-C10**, **MB5-C8**, **MB6-C12**, and **MB7-C8** selectively transport Li^+, Na^+, K^+, and Rb^+/Cs^+ ions, respectively, with transport selectivity well aligned with the intrinsic ion binding affinity of the respective crown ethers. Our findings thus uncover the biocompatible C_{60}-fullerene as an excellent platform to construct synthetic ion transporters with unprecedented custom-designable ion transport selectivity, which could provide a *de novo* basis for rationally designing diverse types of artificial ion transporters with high transport selectivity to support interesting applications within the context of lipid or biomimetic membranes.

METHODS

Typical Reaction Conditions. Malonic acid (520 mg, 5.0 mmol), bromo alcohol (1.99−2.92 g, 11 mmol), and 4-dimethylaminopyridine (244 mg, 2.0 mmol) were dissolved in a mixed solvent of dichloromethane (10 mL) and dimethylformamide (10 mL). After the mixture was cooled to 0 °C using an ice bath, *N*-(3-(dimethylamino)propyl)-*N*′-ethylcarbodiimide hydrochloride (2.90 g, 15 mmol) was added, and the reaction mixture was warmed up overnight with stirring. Removal of solvent *in vacuo* gave the crude product, which was washed using deionized water three times, dried over Na_2SO_4, and then subjected to column chromatography to afford the malonate linker with yields of 30−52%. The obtained linker (628−874 mg, 1.46 mmol), C_{60}-fullerene (105 mg, 0.15 mmol), and CBr_4 (4.84 g, 15 mmol) were dissolved in 1,2-dichlorobenzene (15 mL), to which 1,8-diazabicyclo[5.4.0]undec-7-ene (445 mg, 2.9 mmol) was added dropwise. The reaction mixture was stirred at room temperature for 3 days. Filtration of the reaction mixture gave a dark red solution that was subjected to column chromatography to afford the C_{60}-linker complex with yields of 69−75%. A suspension of the C_{60}-linker complex (224−292 mg, 0.068 mmol), 4′-carboxybenzo-crown (239−356 mg, 0.89 mmol), and K_2CO_3 (246 mg, 1.8 mmol) in dimethylformamide or acetonitrile (15 mL) was heated at 85 °C. Removal of solvent *in vacuo* gave the crude product, which was successively washed with deionized water and methanol three times each to afford **MB**s as dark solids or tarlike heavy oils with yields of 84−96%.

NMR and MALDI-TOF Measurements. NMR spectra were acquired with a Bruker ACF-400 (400 MHz) spectrometer. The solubility of compounds with C12 linkers is only moderate in dimethyl sulfoxide, and chloroform was found to dissolve them well. Deuterated dimethyl sulfoxide (DMSO-d_6, 99.5%) and chloroform ($CDCl_3$, 99.8%) were purchased from Cambridge Isotope Laboratories, Inc., and used as received without further purification. MALDI-TOF mass spectra were acquired with a JMS-S3000 Spiral TOF instrument (JEOL Ltd., Japan) in the positive linear configuration. System parameters were as follows: 20 kV accelerating potential, 250 Hz laser frequency, 500 ns delay time. The matrix was a saturated solution of 1,8,9-trihydroxyanthracene (dithranol) in dichloromethane.

Ion Transport Study and EC_{50} Measurements Using the HPTS Assay. Egg yolk L-α-phosphatidylcholine (EYPC, 1.0 mL, 25 mg/mL in chloroform, Avanti Polar Lipids, USA) was loaded into a round-bottom flask, and the solvent was removed under reduced pressure at 30 °C. After the resulting film was dried under high vacuum overnight at room temperature, the film was hydrated with HEPES buffer solution (1.0 mL, 10 mM HEPES, 100 mM NaCl, pH 7.0) containing the pH-sensitive HPTS dye (1.0 mM) at room temperature for 45 min to give a milky suspension. The mixture was then subject to 10 freeze−thaw cycles: freezing in liquid N_2 for 1 min and heating at 55 °C in a water bath for 2 min. The vesicle suspension was extruded through a polycarbonate membrane (0.1 μm) to produce a homogeneous suspension of large unilamellar vesicles (LUVs) of about 120 nm in diameter with HPTS trapped inside. The extravesicular HPTS dye was separated from the LUVs using size exclusion chromatography (stationary phase, Sephadex G-50, GE Healthcare, USA; mobile phase, 10 mM HEPES buffer with 100 mM NaCl, pH 7.0) and diluted with the mobile phase to yield 5.0 mL of 6.5 mM lipid stock solution. The LUV solution was stored in 4 °C refrigerator until use. The HPTS-containing LUV suspension (30 μL) was added to a HEPES buffer solution (1.96 mL, 10 mM HEPES, 100 mM MCl at pH 8.0, where M^+ = Li^+, Na^+, K^+, Rb^+, Cs^+) to create a pH gradient for ion transport studies. A solution of **MB** in dimethyl sulfoxide or dimethylformamide (those with *n*-C12 linkers) at different concentrations was then injected into the suspension with gentle stirring. Upon addition, the emission of HPTS was immediately monitored at 510 nm with excitations at 403 nm recorded for 300 s using a fluorescence spectrophotometer (Hitachi, Model F-7100, Japan). At 300 s, an aqueous solution of Triton X-100 (20 μL, 20% v/v) was injected to induce the maximum change in dye fluorescence emission. The final transport trace was obtained by normalizing the fluorescence intensity using the equation $I_f = (I_t - I_0)/(I_1 - I_0)$, where I_f = fractional emission intensity, I_t = fluorescence intensity at time *t*, I_1 = fluorescence intensity after addition of Triton X-100, and I_0 = initial fluorescence intensity. The fractional change R_{M^+} was calculated for each curve using the normalized value of I_f at 300 s before the addition of Triton, with the blank set as 0% and that of Triton as 100%. Fitting the fractional transmembrane activity R_{M^+} vs transporter concentration used the Hill equation: $Y = 1/(1 + (EC_{50}/[\mathbf{MB}])^n)$ gave the EC_{50} values.

ASSOCIATED CONTENT

Supporting Information

The Supporting Information is available free of charge at https://pubs.acs.org/doi/10.1021/jacs.0c09655.

Synthetic procedures, a full set of characterization data including ^1H NMR, ^{13}C NMR, and MS, and a complete set of ion transport studies (PDF)

AUTHOR INFORMATION

Corresponding Author

Huaqiang Zeng − *Institute of Advanced Synthesis and Yangtze River Delta Research Institute, Northwestern Polytechnical University, Xi'an, Shaanxi 710072, People's Republic of China*; orcid.org/0000-0002-8246-2000; Email: hqzeng@nwpu.edu.cn

Authors

Ning Li − *The NanoBio Lab, Singapore 138669*; orcid.org/0000-0003-0179-1425

Feng Chen − *The NanoBio Lab, Singapore 138669*

Jie Shen − *The NanoBio Lab, Singapore 138669*

Hao Zhang − *Institute of Advanced Synthesis and Yangtze River Delta Research Institute, Northwestern Polytechnical University, Xi'an, Shaanxi 710072, People's Republic of China*; orcid.org/0000-0002-7961-3322

Tianxiang Wang − *School of Physical & Mathematical Sciences, Nanyang Technological University, Singapore 637371*

Ruijuan Ye − *Institute of Advanced Synthesis and Yangtze River Delta Research Institute, Northwestern Polytechnical University, Xi'an, Shaanxi 710072, People's Republic of China*

Tianhu Li − *Institute of Advanced Synthesis and Yangtze River Delta Research Institute, Northwestern Polytechnical University, Xi'an, Shaanxi 710072, People's Republic of China*

Teck Peng Loh − *Institute of Advanced Synthesis and Yangtze River Delta Research Institute, Northwestern Polytechnical University, Xi'an, Shaanxi 710072, People's Republic of China; School of Physical & Mathematical Sciences, Nanyang Technological University, Singapore 637371;* orcid.org/0000-0002-2936-337X

Yi Yan Yang − *Institute of Bioengineering and Nanotechnology, The Nanos, Singapore 138669;* orcid.org/0000-0002-1871-5448

Complete contact information is available at: https://pubs.acs.org/10.1021/jacs.0c09655

Notes

The authors declare no competing financial interest.

■ ACKNOWLEDGMENTS

This work was supported by the Institute of Advanced Synthesis, Northwestern Polytechnical University, and Nano-Bio Lab (Biomedical Research Council, Agency for Science, Technology and Research, Singapore).

■ REFERENCES

(1) Zaydman, M. A.; Silva, J. R.; Cui, J. Ion Channel Associated Diseases: Overview of Molecular Mechanisms. *Chem. Rev.* **2012**, *112*, 6319.

(2) Cooper, E. C.; Jan, L. Y. Ion channel genes and human neurological disease: Recent progress, prospects, and challenges. *Proc. Natl. Acad. Sci. U. S. A.* **1999**, *96*, 4759.

(3) Gouaux, E.; MacKinnon, R. Principles of Selective Ion Transport in Channels and Pumps. *Science* **2005**, *310*, 1461.

(4) Doyle, D. A.; Cabral, J. M.; Pfuetzner, R. A.; Kuo, A.; Gulbis, J. M.; Cohen, S. L.; Chait, B. T.; MacKinnon, R. The Structure of the Potassium Channel: Molecular Basis of K^+ Conduction and Selectivity. *Science* **1998**, *280*, 69.

(5) Payandeh, J.; Gamal El-Din, T. M.; Scheuer, T.; Zheng, N.; Catterall, W. A. Crystal structure of a voltage-gated sodium channel in two potentially inactivated states. *Nature* **2012**, *486*, 135.

(6) Zhang, X.; Ren, W.; DeCaen, P.; Yan, C.; Tao, X.; Tang, L.; Wang, J.; Hasegawa, K.; Kumasaka, T.; He, J.; Wang, J.; Clapham, D. E.; Yan, N. Crystal structure of an orthologue of the NaChBac voltage-gated sodium channel. *Nature* **2012**, *486*, 130.

(7) Yoder, J. B.; Ben-Johny, M.; Farinelli, F.; Srinivasan, L.; Shoemaker, S. R.; Tomaselli, G. F.; Gabelli, S. B.; Amzel, L. M. Ca^{2+}-dependent regulation of sodium channels NaV1.4 and NaV1.5 is controlled by the post-IQ motif. *Nat. Commun.* **2019**, *10*, 1514.

(8) Gokel, G. W.; Carasel, I. A. Biologically active, synthetic ion transporters. *Chem. Soc. Rev.* **2007**, *36*, 378.

(9) Matile, S.; Vargas Jentzsch, A.; Montenegro, J.; Fin, A. Recent synthetic transport systems. *Chem. Soc. Rev.* **2011**, *40*, 2453.

(10) Zheng, S.-P.; Huang, L.-B.; Sun, Z.; Barboiu, M. Self-assembled Artificial Ion-Channels toward Natural Selection of Functions. *Angew. Chem.* **2020**, DOI: 10.1002/ange.201915287.

(11) Park, S.-H.; Park, S.-H.; Howe, E. N. W.; Hyun, J. Y.; Chen, L.-J.; Hwang, I.; Vargas-Zuñiga, G.; Busschaert, N.; Gale, P. A.; Sessler, J. L.; Shin, I. Determinants of Ion-Transporter Cancer Cell Death. *Chem.* **2019**, *5*, 2079.

(12) Li, H.; Valkenier, H.; Thorne, A. G.; Dias, C. M.; Cooper, J. A.; Kieffer, M.; Busschaert, N.; Gale, P. A.; Sheppard, D. N.; Davis, A. P. Anion carriers as potential treatments for cystic fibrosis: transport in cystic fibrosis cells, and additivity to channel-targeting drugs. *Chem. Sci.* **2019**, *10*, 9663.

(13) Montenegro, J.; Ghadiri, M. R.; Granja, J. R. Ion Channel Models Based on Self-Assembling Cyclic Peptide Nanotubes. *Acc. Chem. Res.* **2013**, *46*, 2955.

(14) Fyles, T. M. How Do Amphiphiles Form Ion-Conducting Channels in Membranes? Lessons from Linear Oligoesters. *Acc. Chem. Res.* **2013**, *46*, 2847.

(15) Otis, F.; Auger, M.; Voyer, N. Exploiting Peptide Nanostructures To Construct Functional Artificial Ion Channels. *Acc. Chem. Res.* **2013**, *46*, 2934.

(16) Gong, B.; Shao, Z. Self-Assembling Organic Nanotubes with Precisely Defined, Sub-nanometer Pores: Formation and Mass Transport Characteristics. *Acc. Chem. Res.* **2013**, *46*, 2856.

(17) Ren, C.; Chen, F.; Ye, R. J.; Ong, Y. S.; Lu, H.; Lee, S. S.; Ying, J. Y.; Zeng, H. Q. Molecular Swings as Highly Active Ion Transporters. *Angew. Chem., Int. Ed.* **2019**, *58*, 8034.

(18) Pedersen, C. J. Cyclic polyethers and their complexes with metal salts. *J. Am. Chem. Soc.* **1967**, *89*, 2495.

(19) Ren, C.; Shen, J.; Zeng, H. Q. Combinatorial Evolution of Fast-Conducting Highly Selective K^+-Channels via Modularly Tunable Directional Assembly of Crown Ethers. *J. Am. Chem. Soc.* **2017**, *139*, 12338.

(20) Feng, W.-X.; Sun, Z.; Zhang, Y.; Legrand, Y.-M.; Petit, E.; Su, C.-Y.; Barboiu, M. Bis-15-crown-5-ether-pillar[5]arene K^+-Responsive Channels. *Org. Lett.* **2017**, *19*, 1438.

(21) Ye, R. J.; Ren, C.; Shen, J.; Li, N.; Chen, F.; Roy, A.; Zeng, H. Q. Molecular Ion Fishers as Highly Active and Exceptionally Selective K^+ Transporters. *J. Am. Chem. Soc.* **2019**, *141*, 9788.

(22) Gokel, G. W.; Negin, S. Synthetic Ion Channels: From Pores to Biological Applications. *Acc. Chem. Res.* **2013**, *46*, 2824.

(23) Meillon, J.-C.; Voyer, N. A Synthetic Transmembrane Channel Active in Lipid Bilayers. *Angew. Chem., Int. Ed. Engl.* **1997**, *36*, 967.

(24) Sun, Z.; Barboiu, M.; Legrand, Y.-M.; Petit, E.; Rotaru, A. Highly Selective Artificial Cholesteryl Crown Ether K^+-Channels. *Angew. Chem., Int. Ed.* **2015**, *54*, 14473.

(25) Gilles, A.; Barboiu, M. Highly Selective Artificial K^+ Channels: An Example of Selectivity-Induced Transmembrane Potential. *J. Am. Chem. Soc.* **2016**, *138*, 426.

(26) Voyer, N.; Robitaille, M. Novel Functional Artificial Ion Channel. *J. Am. Chem. Soc.* **1995**, *117*, 6599.

(27) Otis, F.; Racine-Berthiaume, C.; Voyer, N. How Far Can a Sodium Ion Travel within a Lipid Bilayer? *J. Am. Chem. Soc.* **2011**, *133*, 6481.

(28) Gokel, G. W. Hydraphiles: design, synthesis and analysis of a family of synthetic, cation-conducting channels. *Chem. Commun.* **2000**, 1.

(29) Christy, F. A.; Shrivastav, P. S. Conductometric Studies on Cation-Crown Ether Complexes: A Review. *Crit. Rev. Anal. Chem.* **2011**, *41*, 236.

(30) Steed, J. W. First- and second-sphere coordination chemistry of alkali metal crown ether complexes. *Coord. Chem. Rev.* **2001**, *215*, 171.

(31) Dang, L. X. Mechanism and Thermodynamics of Ion Selectivity in Aqueous Solutions of 18-Crown-6 Ether: A Molecular Dynamics Study. *J. Am. Chem. Soc.* **1995**, *117*, 6954.

(32) Ali, M.; Ahmed, I.; Ramirez, P.; Nasir, S.; Mafe, S.; Niemeyer, C. M.; Ensinger, W. Lithium Ion Recognition with Nanofluidic Diodes through Host−Guest Complexation in Confined Geometries. *Anal. Chem.* **2018**, *90*, 6820.

(33) Liou, C.-C.; Brodbelt, J. S. Determination of orders of relative alkali metal ion affinities of crown ethers and acyclic analogs by the kinetic method. *J. Am. Soc. Mass Spectrom.* **1992**, *3*, 543.

(34) Izatt, R. M.; Bradshaw, J. S.; Nielsen, S. A.; Lamb, J. D.; Christensen, J. J.; Sen, D. Thermodynamic and kinetic data for cation-macrocycle interaction. *Chem. Rev.* **1985**, *85*, 271.

(35) Saha, T.; Hossain, M. S.; Saha, D.; Lahiri, M.; Talukdar, P. Chloride-Mediated Apoptosis-Inducing Activity of Bis(sulfonamide) Anionophores. *J. Am. Chem. Soc.* **2016**, *138*, 7558.

(36) Mondal, D.; Sathyan, A.; Shinde, S. V.; Mishra, K. K.; Talukdar, P. Tripodal cyanurates as selective transmembrane Cl− transporters. *Org. Biomol. Chem.* **2018**, *16*, 8690.

(37) Li, H.; Zhang, B.; Lu, X.; Tan, X.; Jia, F.; Xiao, Y.; Cheng, Z.; Li, Y.; Silva, D. O.; Schrekker, H. S.; Zhang, K.; Mirkin, C. A. Molecular spherical nucleic acids. *Proc. Natl. Acad. Sci. U. S. A.* **2018**, *115*, 4340.
(38) Li, H.; Li, Y.; Xiao, Y.; Zhang, B.; Cheng, Z.; Shi, J.; Xiong, J.; Li, Z.; Zhang, K. Well-Defined DNA−Polymer Miktoarm Stars for Enzyme-Resistant Nanoflares and Carrier-Free Gene Regulation. *Bioconjugate Chem.* **2020**, *31*, 530.
(39) Minami, K.; Okamoto, K.; Harano, K.; Noiri, E.; Nakamura, E. Hierarchical Assembly of siRNA with Tetraamino Fullerene in Physiological Conditions for Efficient Internalization into Cells and Knockdown. *ACS Appl. Mater. Interfaces* **2018**, *10*, 19347.
(40) Stauber, J. M.; Qian, E. A.; Han, Y.; Rheingold, A. L.; Král, P.; Fujita, D.; Spokoyny, A. M. An Organometallic Strategy for Assembling Atomically Precise Hybrid Nanomaterials. *J. Am. Chem. Soc.* **2020**, *142*, 327.
(41) Jones, S. T.; Cagno, V.; Janeček, M.; Ortiz, D.; Gasilova, N.; Piret, J.; Gasbarri, M.; Constant, D. A.; Han, Y.; Vuković, L.; Král, P.; Kaiser, L.; Huang, S.; Constant, S.; Kirkegaard, K.; Boivin, G.; Stellacci, F.; Tapparel, C. Modified cyclodextrins as broad-spectrum antivirals. *Sci. Adv.* **2020**, *6*, eaax9318.
(42) Moore, S. S.; Tarnowski, T. L.; Newcomb, M.; Cram, D. J. Host-guest complexation. 4. Remote substituent effects on macrocyclic polyether binding to metal and ammonium ions. *J. Am. Chem. Soc.* **1977**, *99*, 6398.
(43) Muñoz, A.; Sigwalt, D.; Illescas, B. M.; Luczkowiak, J.; Rodríguez-Pérez, L.; Nierengarten, I.; Holler, M.; Remy, J.-S.; Buffet, K.; Vincent, S. P.; Rojo, J.; Delgado, R.; Nierengarten, J.-F.; Martín, N. Synthesis of giant globular multivalent glycofullerenes as potent inhibitors in a model of Ebola virus infection. *Nat. Chem.* **2016**, *8*, 50.
(44) Tedesco, M. M.; Ghebremariam, B.; Sakai, N.; Matile, S. Modeling the Selectivity of Potassium Channels with Synthetic, Ligand-Assembled π Slides. *Angew. Chem., Int. Ed.* **1999**, *38*, 540.
(45) Sakai, N.; Majumdar, N.; Matile, S. Self-Assembled Rigid-Rod Ionophores. *J. Am. Chem. Soc.* **1999**, *121*, 4294.
(46) Zeng, L. Z.; Zhang, H.; Wang, T.; Li, T. Enhancing K^+ transport activity and selectivity of synthetic K^+ channels via electron-donating effects. *Chem. Commun.* **2020**, *56*, 1211.
(47) Shanzer, A.; Samuel, D.; Kornstein, R. Lipophilic lithium ion carriers. *J. Am. Chem. Soc.* **1983**, *105*, 3815.
(48) Baldessarini, R. J.; Tondo, L.; Davis, P.; Pompili, M.; Goodwin, F. K.; Hennen, J. Decreased risk of suicides and attempts during long-term lithium treatment: a meta-analytic review. *Bipolar Disord.* **2006**, *8*, 625.
(49) Gitlin, M. Lithium side effects and toxicity: prevalence and management strategies. *Int. J. Bipolar Disord.* **2016**, *4*, 27.
(50) Luo, Y.; Marets, N.; Kato, T. Selective lithium ion recognition in self-assembled columnar liquid crystals based on a lithium receptor. *Chem. Sci.* **2018**, *9*, 608.
(51) Criscuolo, F.; Taurino, I.; Stradolini, F.; Carrara, S.; De Micheli, G. Highly-stable Li^+ ion-selective electrodes based on noble metal nanostructured layers as solid-contacts. *Anal. Chim. Acta* **2018**, *1027*, 22.
(52) Suzuki, K.; Yamada, H.; Sato, K.; Watanabe, K.; Hisamoto, H.; Tobe, Y.; Kobiro, K. Design and synthesis of highly selective ionophores for lithium ion based on 14-crown-4 derivatives for an ion-selective electrode. *Anal. Chem.* **1993**, *65*, 3404.
(53) He, Q.; Li, A.; Guo, Y.; Liu, S.; Zhang, Y.; Kong, L. Tribological properties of nanometer cerium oxide as additives in lithium grease. *J. Rare Earths* **2018**, *36*, 209.
(54) Yang, S.; Zhang, F.; Ding, H.; He, P.; Zhou, H. Lithium Metal Extraction from Seawater. *Joule* **2018**, *2*, 1648.
(55) Swain, B. Recovery and recycling of lithium: A review. *Sep. Purif. Technol.* **2017**, *172*, 388.
(56) Kulikov, O. V.; Li, R.; Gokel, G. W. A Synthetic Ion Channel Derived from a Metallogallarene Capsule That Functions in Phospholipid Bilayers. *Angew. Chem., Int. Ed.* **2009**, *48*, 375.
(57) Wang, W.; Li, R.; Gokel, G. W. Membrane-Length Amphiphiles Exhibiting Structural Simplicity and Ion Channel Activity. *Chem. - Eur. J.* **2009**, *15*, 10543.
(58) Carlsson, J.; Åqvist, J. Absolute Hydration Entropies of Alkali Metal Ions from Molecular Dynamics Simulations. *J. Phys. Chem. B* **2009**, *113*, 10255.
(59) Jin, T.; Kinjo, M.; Koyama, T.; Kobayashi, Y.; Hirata, H. Selective Na+ Transport through Phospholipid Bilayer Membrane by a Synthetic Calix[4]arene Carrier. *Langmuir* **1996**, *12*, 2684.
(60) Waldmann, R.; Champigny, G.; Bassilana, F.; Heurteaux, C.; Lazdunski, M. A proton-gated cation channel involved in acid-sensing. *Nature* **1997**, *386*, 173.
(61) Favre, I.; Moczydlowski, E.; Schild, L. On the structural basis for ionic selectivity among Na^+, K^+, and Ca^{2+} in the voltage-gated sodium channel. *Biophys. J.* **1996**, *71*, 3110.
(62) Li, N.; Shen, J.; Ang Gerome, K.; Ye, R. J.; Zeng, H. Q. Molecular Tetrahedrons as Selective and Efficient Ion Transporters via a Two-Station Swing-Relay Mechanism. *CCS Chem.* **2020**, *2*, 2269.
(63) Munkonge, F.; Alton, E. W. F. W.; Andersson, C.; Davidson, H.; Dragomir, A.; Edelman, A.; Farley, R.; Hjelte, L.; McLachlan, G.; Stern, M.; Roomans, G. M. Measurement of halide efflux from cultured and primary airway epithelial cells using fluorescence indicators. *J. Cystic Fibrosis* **2004**, *3*, 171.
(64) Ren, C.; Ding, X.; Roy, A.; Shen, J.; Zhou, S.; Chen, F.; Yau Li, S. F.; Ren, H.; Yang, Y. Y.; Zeng, H. Q. A halogen bond-mediated highly active artificial chloride channel with high anticancer activity. *Chem. Sci.* **2018**, *9*, 4044.
(65) Rex, S. Pore formation induced by the peptide melittin in different lipid vesicle membranes. *Biophys. Chem.* **1996**, *58*, 75.

https://dx.doi.org/10.1021/jacs.0c09655
J. Am. Chem. Soc. 2020, 142, 21082−21090